

# Fast and Robust Two-Qubit Gates with Microwave-Driven Trapped Ions

I. Arrazola,<sup>1</sup> J. Casanova,<sup>2</sup> J. S. Pedernales,<sup>2</sup> Z.-Y. Wang,<sup>2</sup> E. Solano,<sup>1,3</sup> and M. B. Plenio<sup>2</sup>

<sup>1</sup>*Department of Physical Chemistry, University of the Basque Country UPV/EHU, Apartado 644, 48080 Bilbao, Spain*

<sup>2</sup>*Institute for Theoretical Physics and IQST, Albert-Einstein-Allee 11, Universität Ulm, D-89069 Ulm, Germany*

<sup>3</sup>*IKERBASQUE, Basque Foundation for Science, Maria Diaz de Haro 3, 48013 Bilbao, Spain*

We propose a pulsed dynamical decoupling protocol to be used as the generator of tunable, fast, and robust quantum phase gates between two microwave-driven hyperfine qubits in ion traps. The gate scheme consists of a suitably designed sequence of  $\pi$ -pulses acting on the ions which seat along a magnetic field gradient. Unlike previous approaches, the proposed gate does not rely on the spectroscopic discrimination of a single vibrational mode to act as a quantum bus between the two trapped ions. Instead, in our design, the two vibrational modes in the axial direction of the ion chain are forced to cooperate under the influence of the externally applied microwave driving. In this manner, the gate speed can be significantly increased. Furthermore, our scheme is demonstrated to be robust against the dominant noise sources, which are errors on the magnetic field and microwave pulse intensities as well as motional heating, leading to fast and high-fidelity two-qubit gates. Our detailed numerical simulations, including realistic experimental considerations, show that with state-of-the-art trapped-ion technology, entangling gates with fidelities above 99.9% can be achieved in tens of microseconds.

## I. INTRODUCTION

Entangling gates, faster than decoherence rates and performing with high accuracy, are crucial to quantum technologies [1]. Trapped-ion systems [2, 3] are one of the strong candidate platforms to implement quantum computers and quantum simulators [4–7] in a systematic manner, allowing the execution of quantum algorithms capable of beating classical computers. In terms of speed and accuracy, laser control techniques have provided the best entangling gates in ion traps, reaching two-qubit gates that run in microseconds and have fidelities larger than 99.9% [8, 9]. In addition, entanglement of up to 14 ions has been achieved [10]. However, it is unclear whether technological improvements of the laser control elements alone will be sufficient to scale these systems up to sizes that are computationally relevant, as the technological challenges in setting up and controlling multiple laser sources seem daunting.

In the last years, an alternative route that relies on the microwave quantum control of trapped ions in the presence of a strong magnetic field gradient has been proposed [11], and it is now actively pursued in several laboratories [12, 13]. Substituting lasers by microwaves is appealing from an experimental point of view, as they represent a mature technology that can be controlled with relative ease. Microwave control elements are manipulated entirely with electronic methods, they enjoy greater stability than laser systems, and are sufficiently cheap and small to be integrated in the trap electrodes [14]. More importantly, having full control of the trapped-ion system exclusively with microwave radiation, circumvents the necessity of employing optical transitions with a sizeable spontaneous decay probability, which damage the fidelity of quantum operations [15]. Two approaches to microwave control of trapped ions are usually considered. On the one hand, the manipulation can be done with far-field microwave radiation and the assistance of a static magnetic field gradient [11, 16]. The magnetic field gradient provides spatial field variations on the size of the wave packet of the ion, which

is necessary to generate the qubit-motion coupling that acts as a bus between the qubits. On the other hand, ions can be controlled with the near-field of microwave radiation, which naturally provides the required spatial field variations without the need to add a static magnetic field gradient [17, 18]. In both cases, magnetically sensitive states are required to be used as part of the qubit state, which leads to decoherence due to unavoidable magnetic field fluctuations. In order to protect the qubit from such uncontrolled fluctuations, both approaches can and need to be combined with dynamical decoupling techniques by redefining the qubit in a dressed state that is continuously driven [19, 20] (for an equivalent technique in laser-based trapped ions, see [21] or more recently for quantum simulation purposes [22, 23]). Following this method, encouraging experimental results have been achieved for both, the far-field and the near-field approaches, reaching two-qubit gate fidelities of 98.5% [24] and 99.7% [14], respectively. In both cases, these high fidelities were demonstrated for gate times on the order of milliseconds. Although these experimental results admit technical improvements that could increase their velocities, e.g. by increasing the magnetic field gradient, they are limited by design to gate times that are several orders of magnitude the oscillation period of the ion chain. This is because, both in laser- or microwave-based schemes, qubit-qubit interactions are mediated by a single motional mode acting as a quantum bus, which needs to be spectroscopically discriminated from the rest [25–27]. To guarantee this possibility, the qubit-motion coupling strength should be much smaller than the oscillation frequency of the modes to be neglected, which in turn imposes a limit on the speed of the resulting gate. Attempts to accelerate the gate by increasing the qubit-motion coupling lead to off-resonant coupling that result in a decline of the gate fidelity. Therefore, designing gates that act in time scales comparable with the oscillation period of the ions or faster, necessarily requires involving the effect of all vibrational modes. In this context, gates based on continuous driving schemes do not seem very promising as the incommensurability of the involved oscilla-

tion frequencies [28] excludes the existence of a time at which all modes are simultaneously decoupled from the qubits.

In this article, we propose a scheme leading to fast and high-fidelity two-qubit gates through a specifically designed sequence of microwave  $\pi$ -pulses acting on top of a magnetic field gradient. Our method employs the two vibrational modes in the axial direction of the two-ion chain leading to gate times around the inverse of the trap frequency. On top of that, the sequence is designed with symmetry considerations, which enhance the quantum coherence of the qubits and protect them from uncontrolled noise sources. The fast speed and robustness of our pulsed dynamical decoupling scheme results in two-qubit gates of high fidelity even in presence of motional heating. We validate our ideas with detailed numerical simulations that show that state-of-the-art trapped-ion technology should allow for two-qubit gates fast enough to be incorporated in scalable microwave-driven schemes. The realization of such fast and robust two-qubit gates will pave the way for scalable digital quantum simulators and quantum computers with trapped ions.

Our work is organised as follows: In section II, we present the target system and the method when working under ideal conditions. In section III, we introduce the microwave sequence we will use to achieve the proposed two-qubit gates. Section IV demonstrates the performance of our method when realistic experimental conditions are included in the model.

## II. THE MODEL

We consider a setup consisting of two  $^{171}\text{Yb}^+$  ions in a microwave quantum computer module [29]. For each ion, we define a quantum bit (qubit) between the lowest energy state  $|g\rangle \equiv \{F=0, m_F=0\}$  and the first excited state with positive magnetic moment  $|e\rangle \equiv \{F=1, m_F=1\}$  in the hyperfine manifold, see Fig. 1. The conditions under which transitions to other hyperfine levels can be safely neglected are covered in appendix A. The motion of different ions is coupled via direct Coulomb interaction and can be collectively described by two harmonic normal modes in each of the three spatial dimensions. In the following, we will restrict our analysis to the normal modes in the axial direction  $\hat{z}$ , namely the center-of-mass (com) and the breathing modes, which are independent of the radial ones. That is, we assume that the magnetic field gradient in the radial direction is negligible compared to that in the axial direction. This configuration is described by the Hamiltonian ( $\hbar=1$ )

$$\begin{aligned} H = & [\omega_e + \gamma B(z_1)]|e\rangle\langle e|_1 + \omega_g|g\rangle\langle g|_1 \\ & + [\omega_e + \gamma B(z_2)]|e\rangle\langle e|_2 + \omega_g|g\rangle\langle g|_2 \\ & + \nu_1 a^\dagger a + \nu_2 c^\dagger c. \end{aligned} \quad (1)$$

Here,  $\gamma$  relates to the electronic gyromagnetic ratio  $\gamma_e$  as  $\gamma \simeq \frac{\gamma_e}{2} = (2\pi) \times 1.4 \text{ MHz/G}$ ,  $a(a^\dagger)$  and  $c(c^\dagger)$  are the bosonic annihilation(creation) operators of the motional modes, which

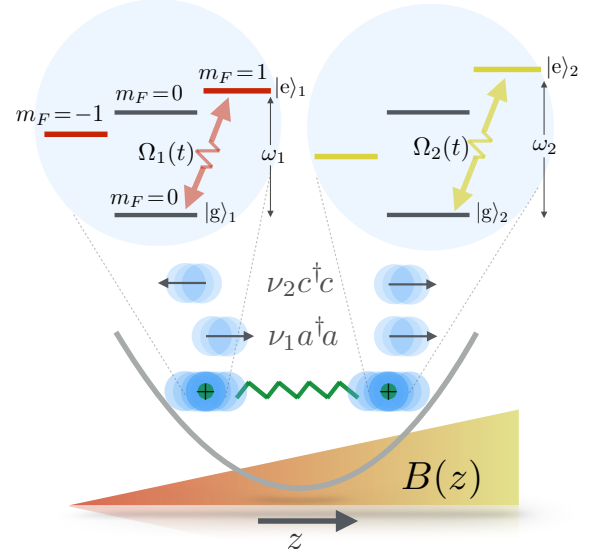


FIG. 1: A scheme of the considered configuration. The hyperfine levels of two  $^{171}\text{Yb}^+$  ions are shown. Because of the applied magnetic field gradient  $B(z)$  the degeneracy of the  $F=1$  manifold is removed and the levels  $\{F=1, m_F=\pm 1\}$  of both ions are separated in energy from the  $\{F=1, m_F=0\}$  by an amount  $\pm\gamma B(z_i)$  respectively.

have frequencies  $\nu_1 = \nu$  and  $\nu_2 = \sqrt{3}\nu$ , respectively [28]. Typical values for  $\nu/(2\pi)$  range from around a hundred of kilohertz to one or two megahertz, and  $B(z_j)$  is the magnetic field at the position of ion  $j$ . We consider a magnetic field gradient that leads to a linearly growing  $B(z_j)$  term,  $\partial B/\partial z = g_B$ . Then, expressing the ion coordinates in terms of the vibrational normal modes [28] and suitably shifting the zero-point energy of the qubits, the Hamiltonian in Eq. (1) can be rewritten as

$$\begin{aligned} H = & \frac{\omega_1}{2}\sigma_1^z + \Delta_1(b + b^\dagger)\sigma_1^z - \Delta_2(c + c^\dagger)\sigma_1^z \\ & + \frac{\omega_2}{2}\sigma_2^z + \Delta_1(b + b^\dagger)\sigma_2^z + \Delta_2(c + c^\dagger)\sigma_2^z \\ & + \nu_1 b^\dagger b + \nu_2 c^\dagger c, \end{aligned} \quad (2)$$

where the operators of the com mode have been redefined as  $b = a + \alpha$ , with  $\alpha = 2\Delta_1/\nu_1$ ,  $\Delta_m = \frac{\gamma g_B}{4} \sqrt{\frac{\hbar}{M\nu_m}}$  being the coupling strength between the qubits and the  $m$ -th motional mode, and  $M$  the mass of each ion. The qubit energy splittings are  $\omega_j = \omega_e - \omega_g - 2\alpha\Delta_1 + \gamma B_j$ , where  $B_j \equiv B(z_j^0)$  is the magnetic field on the equilibrium position of the  $j$ -th ion. For a detailed derivation of Hamiltonian in Eq. (2), please refer to Ref. [30].

In presence of the magnetic field gradient  $g_B$ , the energy splitting of the two ion-qubits differs by  $\omega_2 - \omega_1 = \gamma g_B \Delta z$ , where  $\Delta z$  is the distance between the equilibrium positions of the ions. Later, we will see that  $\omega_2 - \omega_1 = \gamma g_B \left(\frac{2e^2}{4\pi\epsilon_0 M \nu^2}\right)^{1/3}$  is a quantity on the order of tens of megahertz for the parameters considered in this work. This energy difference combined with a specifically designed microwave-pulse sequence to efficiently cancel crosstalk effects (see Sec. IV) will allow us to address individually each qubit. We consider a bichromatic

electromagnetic field of frequencies  $\omega_j$  and phases  $\phi_j$  as described by the Hamiltonian

$$H_c = \Omega_1(t)(\sigma_1^x + \sigma_2^x) \cos(\omega_1 t - \phi_1) + \Omega_2(t)(\sigma_1^x + \sigma_2^x) \cos(\omega_2 t - \phi_2). \quad (3)$$

Under the influence of such microwave control fields our system Hamiltonian would be given by

$$H^I(t) = \Delta_1(b e^{-i\nu_1 t} + b^\dagger e^{i\nu_1 t})\sigma_1^z - \Delta_2(c e^{-i\nu_2 t} + c^\dagger e^{i\nu_2 t})\sigma_1^z + \Delta_1(b e^{-i\nu_1 t} + b^\dagger e^{i\nu_1 t})\sigma_2^z + \Delta_2(c e^{-i\nu_2 t} + c^\dagger e^{i\nu_2 t})\sigma_2^z + \frac{\Omega_1(t)}{2}(\sigma_1^+ e^{i\phi_1} + \sigma_1^- e^{-i\phi_1}) + \frac{\Omega_2(t)}{2}(\sigma_2^+ e^{i\phi_2} + \sigma_2^- e^{-i\phi_2}).$$

The Hamiltonian above is posed in a rotating frame with respect to  $H_0 = \nu_1 b^\dagger b + \nu_2 c^\dagger c + \frac{\omega_1}{2}\sigma_1^z + \frac{\omega_2}{2}\sigma_2^z$ . The non-resonant components of the microwave driving have been eliminated under the rotating-wave approximation (RWA), whose validity will be confirmed by detailed numerical simulations using the first-principle Hamiltonian. In this respect, we want to remark that terms that rotate at a rate similar to  $2\omega_j$  (which corresponds to a frequency of tens of gigahertz for the  $^{171}\text{Yb}^+$  ion, see for example [31]) can be safely neglected by invoking the RWA, see appendix A. The slower frequencies rotating at a rate of  $|\omega_2 - \omega_1|$  (on the order of tens of MHz for our simulated conditions) lead to off-resonant couplings and require a specific treatment covered in Section IV.

The last line in Eq. (4) includes the resonant components of the microwave driving. In order to provide a clear picture of their action, we move to a rotating frame w.r.t. the driving terms  $\frac{\Omega_1(t)}{2}(\sigma_1^+ e^{i\phi_1} + \sigma_1^- e^{-i\phi_1}) + \frac{\Omega_2(t)}{2}(\sigma_2^+ e^{i\phi_2} + \sigma_2^- e^{-i\phi_2})$ . Now by taking into account that the Rabi frequencies will be switched on and off, i.e. the microwave driving will be applied stroboscopically in the form of  $\pi$ -pulses, the Hamiltonian reads

$$H^I(t) = f_1(t)\sigma_1^z[\Delta_1 b e^{-i\nu_1 t} - \Delta_2 c e^{-i\nu_2 t} + \text{H.c.}] + f_2(t)\sigma_2^z[\Delta_1 b e^{-i\nu_1 t} + \Delta_2 c e^{-i\nu_2 t} + \text{H.c.}], \quad (5)$$

where the modulation functions  $f_j(t)$  take the values  $\pm 1$  depending on the number of  $\pi$ -pulses that has been applied to the  $j$ -th ion. More specifically, when an even number of pulses has been applied we have  $f_j = 1$ , while an odd number leads to  $f_j = -1$ .

The idealised description in Eq. (5) assumes that  $\pi$ -pulses are applied instantaneously, which is a good approximation if the Rabi frequencies  $\Omega_1$  and  $\Omega_2$  are much larger than any other frequency (i.e.  $\Delta_{1,2}$  and  $\nu_{1,2}$ ) in Eq. (5). Nevertheless, in order to match realistic experimental conditions, our numerical simulations will consider finite pulses in the form of top-hat functions that require a time  $t_\pi = \frac{\pi}{\Omega}$  to perform a  $\pi$ -rotation.

The Schrödinger equation corresponding to Hamiltonian (5) is analytically solvable leading to the propagator

$$U(t) = U_s(t)U_c(t), \quad (6)$$

where

$$U_s(t) = \exp \left\{ -i [\Delta_1 b G_{11}(t) - \Delta_2 c G_{12}(t) + \text{H.c.}] \sigma_1^z - i [\Delta_1 b G_{21}(t) + \Delta_2 c G_{22}(t) + \text{H.c.}] \sigma_2^z \right\}, \quad (7)$$

and

$$U_c(t) = \exp [i\varphi(t)\sigma_1^z\sigma_2^z]. \quad (8)$$

The  $G_{jm}(t)$  functions in Eq. (S18) are

$$G_{jm}(t) = \int_0^t dt' f_j(t') e^{-i\nu_m t'}, \quad (9)$$

while the achieved phase  $\varphi(t)$  in Eq. (8) can be expressed as

$$\varphi(t) = \left( \frac{\Delta_1}{\nu} \right)^2 [\tilde{\varphi}_1(t) - \frac{1}{3\sqrt{3}} \tilde{\varphi}_2(t)] = \left( \frac{\Delta_1}{\nu} \right)^2 \tilde{\varphi}(t), \quad (10)$$

where

$$\tilde{\varphi}_m(t) = \nu_m^2 \Im \int_0^t dt' [f_1(t') G_{2m}(t') + f_2(t') G_{1m}(t')] e^{i\nu_m t'}, \quad (11)$$

$\Im$  been the imaginary part of the subsequent integral. Moreover, one can demonstrate that, at the end of the sequence, the quantity  $\tilde{\varphi}(t)$  does not depend on the values of  $\Delta_{1,2}$  and  $\nu_{1,2}$  but on the ratio between the mode frequencies which in our case is  $\nu_2/\nu_1 = \sqrt{3}$ . For more details see [30]. Hence, the study of  $\tilde{\varphi}(t)$  appears to be convenient because it covers all situations regardless of the value of the parameters  $\Delta_{1,2}$  and  $\nu_{1,2}$ . Then, the actual phase  $\varphi(t)$  is retrieved by multiplying  $\tilde{\varphi}(t)$  with  $\left( \frac{\Delta_1}{\nu} \right)^2$  according to Eq. (10). In the same manner one can find that, when finishing the sequence,  $\nu_m G_{jm}(t)$  is only dependent on the ratio  $\nu_2/\nu_1$ .

From the solution in Eq. (6), it is clear that a  $\pi$ -pulse sequence of duration  $t_{\text{gate}}$ , satisfying conditions

$$G_{jm}(t_{\text{gate}}) = 0, \quad \varphi(t_{\text{gate}}) \neq 0, \quad (12)$$

would result in a phase gate between the two qubits, while leaving at the end of the process the internal hyperfine degrees of freedom of the ions decoupled from the motion. To accomplish these two conditions, we will design a specific microwave pulse sequence that, in addition, will eliminate the dephasing noise due to magnetic field fluctuations or frequency offsets on the registers. Note that, if the latter are not averaged out, they would spoil the generation of a high-fidelity two-qubit gate.

### III. THE MICROWAVE SEQUENCE

We propose to use variations of the adaptive XY- $n$  (AXY- $n$ ) family of decoupling sequences introduced in Ref. [32] in the context of nanoscale nuclear magnetic resonance with nitrogen vacancy centers in diamond [33–37]. The AXY- $n$  sequence belongs to the set of dynamical decoupling control techniques that extend the coherence time of qubits in the presence of coloured noise, by suppressing the effect of their interaction with the environment. Unlike most other pulsed dynamical decoupling schemes, see different examples

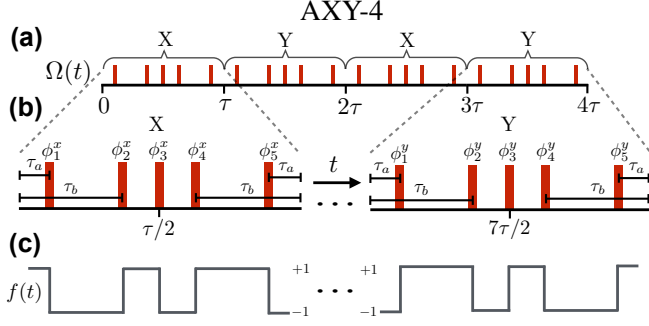


FIG. 2: (a) Pulse sequence including 4 blocks in a AXY-4 configuration. Each block is a composite pulse including 5  $\pi$ -pulses with tunable distances between them. (b) Zoom on the first composite X and Y pulses, where the internal symmetry imposed by the time delays  $\tau_a$  and  $\tau_b$  is shown, together with the corresponding pulse-phases according to Eq. (3). (c) Modulation function associated with the composite pulses above.

at [38], the AXY- $n$  sequence consists of a set of non-equally separated  $\pi$ -pulses, where the interpulse spacing can be tuned while the whole sequence remains robust against errors such as frequency detunings and intensity fluctuations in the microwave control field [32]. This versatility will allow us to design a sequence that meets the conditions in Eq. (12), and therefore not only decouples the qubits from the environment but also results in the performance of a two-qubit phase gate.

The AXY- $n$  sequence consists of  $n$  blocks of 5  $\pi$ -pulses each, as depicted in Fig. 2 for the case of AXY-4. Each  $\pi$ -pulse is applied along an axis in the  $x$ - $y$  plane that is rotated an angle  $\phi$  with respect to the  $x$  axis. Note that this is the pulse phase ( $\phi_1$  or  $\phi_2$ ) that appears in Eq. (3) for the first and second ions, respectively.

We define two blocks: the X block, which consists of 5 rotations along the axes corresponding to  $\vec{\phi}^x \equiv \{\phi_1^x, \phi_2^x, \phi_3^x, \phi_4^x, \phi_5^x\} = \{\frac{\pi}{6}, \frac{\pi}{2}, 0, \frac{\pi}{2}, \frac{\pi}{6}\} + \zeta$ , with  $\zeta$  an arbitrary constant phase, and the Y block, which performs the rotations along the same axes shifted by a phase of  $\pi/2$ , i.e.  $\vec{\phi}^y = \{\frac{\pi}{6} + \frac{\pi}{2}, \pi, \frac{\pi}{2}, \pi, \frac{\pi}{6} + \frac{\pi}{2}\} + \zeta$ . The sequence then consists of a series of  $n$  consecutive X and Y blocks. For example, an AXY-4 sequence would be XYXY, while an AXY-8 sequence is built by nesting 2 AXY-4 blocks with an additional symmetry consideration, more specifically the latter is XXXYXXYX, see [32]. The time distribution of pulses inside each block is identical. As illustrated in Fig. 2(b), each block is symmetric and has a duration  $\tau$ , where a  $\pi$ -pulse is applied. Therefore, within a five pulse block, X or Y, the time of application of the first and second pulses,  $\tau_a$  and  $\tau_b$ , respectively, together with  $\tau$  completely define the whole sequence.

The adaptability of the method is given by the freedom to set these three parameters, which need only to fulfill the condition  $\tau_a < \tau_b < \tau/2$ . It can be shown that at the end of any AXY- $n$  sequence of length  $n\tau$  for an even integer  $n$ , the function  $G_{jm}(n\tau)$ , see Eq. (9), is identically zero for values of  $\tau$

that are a multiple of the oscillation period of mode  $m$ , that is to say for  $\nu_m\tau = 2\pi r$  with  $r = 1, 2, 3, \dots$  (see appendix B for a demonstration). This means that a qubit can be left in a product state with a specific motional mode, at times  $n\tau$ , just by guaranteeing that the sequence is composed of blocks of a length that matches a multiple of the oscillation period of such a mode, regardless of the values of  $\tau_a$  and  $\tau_b$ . Unfortunately, the two motional modes in our system have incommensurable oscillation frequencies (note that  $\nu_1 = \nu$  and  $\nu_2 = \sqrt{3}\nu$ ), which leads to the impossibility of finding a value of  $\tau$  that by itself results in having the qubit in a product state with respect to both modes at the same time. However, by suitably adapting parameters  $\tau_a$  and  $\tau_b$ , we can find a sequence of pulses that, when it finishes, leaves the qubit in a product state with both motional modes.

We will design an AXY-4 sequence of a duration  $4\tau$  such that  $\tau = 2\pi r/\nu_1$ , which makes  $G_{j1}(4\tau) = 0$  for any choice of  $\tau_a$  and  $\tau_b$ , and we will numerically look for the values of  $\tau_a$  and  $\tau_b$  that minimise  $G_{j2}(4\tau)$ . In addition, and for the sake of simplicity in the presentation of this part, we consider that  $f_1(t) = f_2(t)$ , i.e. the same sequence will be simultaneously applied to both qubits, which leads to  $G_{1m} = G_{2m}$ . However, we want to note that when real pulses are considered, we will not use simultaneous driving in order to efficiently eliminate crosstalk effects and to result in a better performance of the method (see next section IV). In Fig. 3(a) we give a 2 dimensional colour plot of  $G_{j2}(4\tau)$  for  $\tau = 2\pi/\nu_1$  for all possible combinations of  $\tau_a$  and  $\tau_b$ . The dark blue regions represent the choice of values of  $\tau_a$  and  $\tau_b$  that minimise the  $G_{j2}(4\tau)$  functions. This, therefore, results in a valid sequence for a two-qubit phase gate. At Fig. 3(b), we give the corresponding value for  $\tilde{\varphi}(4\tau)$ , see Eq. (11), of the resulting two-qubit gate. In Figs. 3(c), 3(d) and 3(e), 3(f) the same procedure is shown for the cases  $\tau = 2 \times 2\pi/\nu_1$  and  $\tau = 3 \times 2\pi/\nu_1$ , respectively. That is, for values  $r = 2$  and  $r = 3$ , obtaining several combinations of  $\tau_a$  and  $\tau_b$  that result in a phase gate. We remark that, for values of  $\tau$  that are higher multiples of  $2\pi/\nu_1$ , larger phases are obtained.

Finally, as it is shown in Eq. (10) to recover the actual phase, we should multiply  $\tilde{\varphi}(4\tau)$  by the frequency ratio,

$$\left(\frac{\Delta_1}{\nu}\right)^2 = \frac{\hbar\gamma^2 g_B^2}{16M\nu^3}, \quad (13)$$

which depends on the values of  $\nu$  and  $g_B$ . In conclusion, the speed of the gate and the actual phase  $\varphi$  will directly depend on these two parameters.

#### IV. TAILORED SEQUENCES AND RESULTS

We will benchmark the performance of our microwave pulsed scheme by means of detailed numerical simulations. The total Hamiltonian governing the dynamics is  $H + H_c$ , where  $H$  and  $H_c$  are given in Eqs. (2) and (3) respectively. In a rotating frame with respect to  $H_0$  and after neglecting

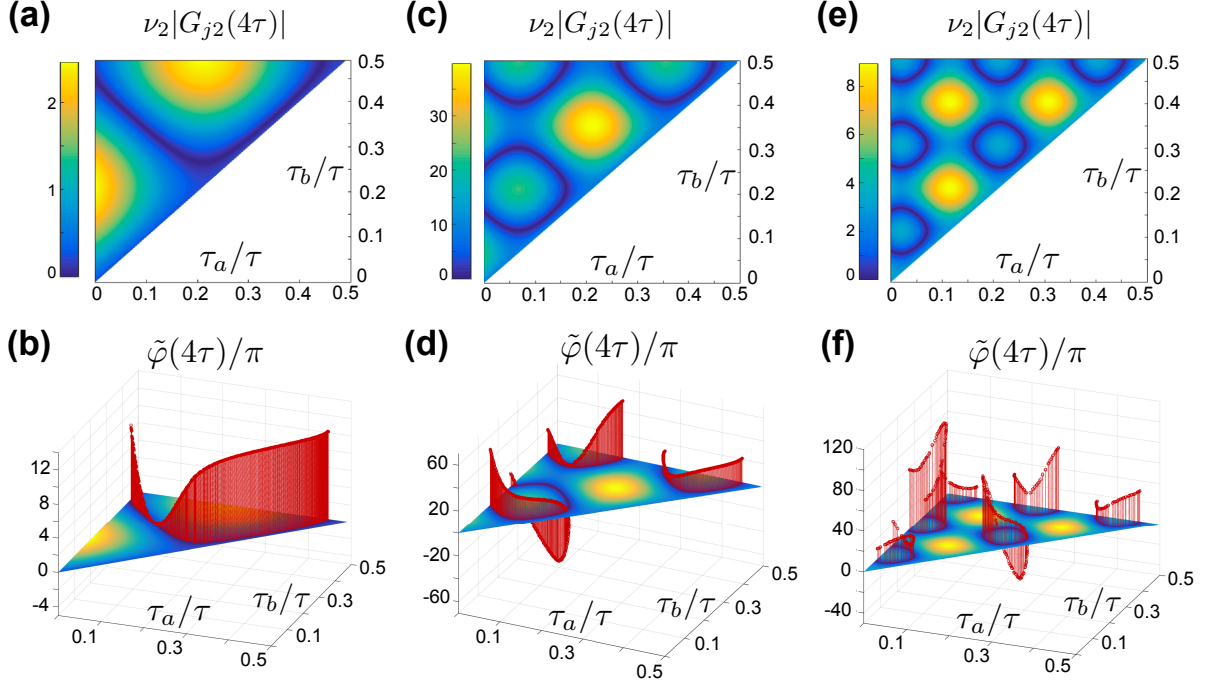


FIG. 3: The value  $G_{j2}(t)$  at the end of an AXY-4 sequence as a function of  $\tau_a$  and  $\tau_b$  ( $\tau_a < \tau_b < \tau/2$ ), for the cases where (a):  $\tau = 1 \times 2\pi/\nu_1$ , (c):  $\tau = 2 \times 2\pi/\nu_1$ , (e):  $\tau = 3 \times 2\pi/\nu_1$ . The dark blue regions show the values of  $\tau_a$  and  $\tau_b$  that correspond to a complete decoupling of the qubits and the modes at the end of the sequence. The phases  $\tilde{\varphi}(t)$  obtained with these sequences are shown in (b),(d),(f) and represented by the red pannels.

terms that rotate at a speed of tens of GHz (see appendix A for details), the effective Hamiltonian reads

$$\begin{aligned}
 H^I(t) = & \Delta_1(b e^{-i\nu_1 t} + b^\dagger e^{+i\nu_1 t})\sigma_1^z - \Delta_2(c e^{-i\nu_2 t} + c^\dagger e^{+i\nu_2 t})\sigma_2^z \\
 & + \Delta_1(b e^{-i\nu_1 t} + b^\dagger e^{+i\nu_1 t})\sigma_2^z - \Delta_2(c e^{-i\nu_2 t} + c^\dagger e^{+i\nu_2 t})\sigma_1^z \\
 & + \frac{\Omega_1(t)}{2}\sigma_1^{\phi_1} + \frac{\Omega_1(t)}{2}(\sigma_2^+ e^{i\delta_2 t} e^{i\phi_1} + \text{H.c.}) \\
 & + \frac{\Omega_2(t)}{2}\sigma_2^{\phi_2} + \frac{\Omega_2(t)}{2}(\sigma_1^+ e^{i\delta_1 t} e^{i\phi_2} + \text{H.c.}). \quad (14)
 \end{aligned}$$

Here,  $\sigma_j^{\phi_j} = \sigma_j^+ e^{i\phi_j} + \sigma_j^- e^{-i\phi_j}$ , and the last two lines contain both the resonant terms giving rise to the  $\pi$ -pulses, i.e.  $\frac{\Omega_1(t)}{2}\sigma_1^{\phi_1}$  and  $\frac{\Omega_2(t)}{2}\sigma_2^{\phi_2}$ , as well as crosstalk contributions of each  $\pi$ -pulse on the off-resonant ion. The latter are  $\frac{\Omega_1(t)}{2}(\sigma_2^+ e^{i\delta_2 t} e^{i\phi_1} + \text{H.c.})$  and  $\frac{\Omega_2(t)}{2}(\sigma_1^+ e^{i\delta_1 t} e^{i\phi_2} + \text{H.c.})$ , where  $\delta_2 = -\delta_1 = \omega_2 - \omega_1$ . We use Eq. (14) as the starting point of our simulations without any further assumptions. In addition, our numerical simulations include noise contributions coming from motional decoherence processes and errors on the Rabi frequencies of the driving microwave fields, and on the resonance frequencies,  $\omega_{1,2}$ , of the ions.

To get rid of crosstalk effects, we use a decoupling scheme acting non simultaneously on both ions that, at the same time, meets conditions in Eqs. (12), and give rise to a tunable phase gate between the ions. In this respect, one can demonstrate

that a term like

$$\frac{\Omega_1(t)}{2}\sigma_1^{\phi_1} + \frac{\Omega_1(t)}{2}(\sigma_2^+ e^{i\delta_2 t} e^{i\phi_1} + \text{H.c.}), \quad (15)$$

for a final time  $t_\pi^{(1)} = \frac{\pi}{\Omega_1}$ , i.e. the required time for a  $\pi$ -pulse on the first ion, has the associate propagator

$$U_{t_\pi^{(1)}} = e^{-i\frac{\Omega_1}{2}\sigma_1^{\phi_1} t_\pi} e^{i\frac{\delta_2}{2}\sigma_2^z t_\pi}, \quad (16)$$

if and only if the Rabi frequency  $\Omega_1$  satisfies

$$\Omega_1 = \frac{\delta_2}{\sqrt{4k^2 - 1}}, \text{ with } k \in \mathbb{N}. \quad (17)$$

See appendix C for a demonstration of this. In the same manner, the term  $\frac{\Omega_2(t)}{2}\sigma_2^{\phi_2} + \frac{\Omega_2(t)}{2}(\sigma_1^+ e^{i\delta_1 t} e^{i\phi_2} + \text{H.c.})$  gives rise to  $U_{t_\pi^{(2)}} = e^{-i\frac{\Omega_2}{2}\sigma_2^{\phi_2} t_\pi} e^{i\frac{\delta_1}{2}\sigma_1^z t_\pi}$  under the conditions  $t_\pi^{(2)} = \frac{\pi}{\Omega_2}$  and  $\Omega_2 = |\delta_1|/\sqrt{4k^2 - 1}$ , with  $k \in \mathbb{N}$ . Hence, when the microwave driving is applied non-simultaneously over the registers, one can clearly argue that a  $\pi$ -pulse on the first ion induces a dephasing-like propagator on the second ion (i.e.  $e^{i\frac{\delta_2}{2}\sigma_2^z t_\pi}$ ) and vice versa. Therefore, our decoupling sequence has to be designed in a manner that it eliminates such undesired contribution.

Our target sequence is depicted in Fig. 4(a), where one has to select the parameters  $\tau_{a,b}$  and  $\Delta t$ . While  $\tau_{a,b}$  define the sequence acting on the first ion, a temporal translation





TABLE I: Infidelities for two-qubit gates with different phases after the application of 20 imperfect microwave pulses on each ion, according to the AXY-4 protocol. We calculate the infidelities for several initial states including some entangled ones (first column up to a normalisation factor) and different experimental conditions as described in the main text. More specifically, in each box we denote the values for the employed magnetic field gradient  $g_B$ , the frequency of the com mode  $\nu$ , and the required time for the gate  $t_{\text{gate}}$ . We focus in  $\pi/4$  and  $\pi/8$  entangling phase gates, however our method is general and can achieve any evolving phase.

Infidelity ( $\times 10^{-4}$ )	$\exp(i\frac{\pi}{4}\sigma_1^z\sigma_2^z)$ $g_B = 150 \text{ T/m}$ $\nu/(2\pi) = 150 \text{ kHz}$ $t_{\text{gate}} = 80 \mu\text{s}$	$\exp(i\frac{\pi}{8}\sigma_1^z\sigma_2^z)$ $g_B = 150 \text{ T/m}$ $\nu/(2\pi) = 150 \text{ kHz}$ $t_{\text{gate}} = 80 \mu\text{s}$	$\exp(i\frac{\pi}{4}\sigma_1^z\sigma_2^z)$ $g_B = 300 \text{ T/m}$ $\nu/(2\pi) = 220 \text{ kHz}$ $t_{\text{gate}} = 36.3 \mu\text{s}$	$\exp(i\frac{\pi}{8}\sigma_1^z\sigma_2^z)$ $g_B = 300 \text{ T/m}$ $\nu/(2\pi) = 220 \text{ kHz}$ $t_{\text{gate}} = 36.3 \mu\text{s}$
$ g\rangle \otimes ( g\rangle +  e\rangle)$	1.172	0.128	2.060	0.144
$( g\rangle +  e\rangle) \otimes ( g\rangle +  e\rangle)$	2.229	0.136	4.905	0.304
$ g\rangle \otimes ( g\rangle + i e\rangle) +  e\rangle \otimes  e\rangle$	3.052	0.116	5.899	0.371
$ e\rangle \otimes ( g\rangle - i e\rangle) +  g\rangle \otimes  g\rangle$	4.631	0.172	5.946	0.413
$ e\rangle \otimes ( g\rangle - i e\rangle) +  g\rangle \otimes ( g\rangle + i e\rangle)$	3.250	0.110	4.635	0.293

We have calculated gate infidelity for the following situations. Firstly, we consider the numerical simulation of the gates  $\exp(i\frac{\pi}{4}\sigma_1^z\sigma_2^z)$  and  $\exp(i\frac{\pi}{8}\sigma_1^z\sigma_2^z)$  in a time of  $80 \mu\text{s}$  when there is a magnetic field gradient of  $150 \frac{\text{T}}{\text{m}}$  (see for example [24]). Here, we designed the microwave sequence such that  $\tau = 2\pi r/\nu_1$  with  $r = 3$  (see section III) leading to a gate time which is 12 times the oscillation period of the com mode. The other relevant parameters are com and breathing mode frequencies of  $\nu_1 = (2\pi) \times 150 \text{ kHz}$ ,  $\nu_2 = (2\pi) \times \sqrt{3} 150 \text{ kHz}$ , and a  $\pi$ -pulse time of  $\approx 75 \text{ ns}$  that implies a Rabi frequency for the microwave driving field of  $\Omega_1 = \Omega_2 = \Omega \approx (2\pi) \times 6.63 \text{ MHz}$ . The difference between the resonance energies for the qubits is  $\omega_2 - \omega_1 = (2\pi) \times 25.7 \text{ MHz}$ , while we have chosen the  $\Delta t$  parameter, see Fig. 4, as 1.05 times the value of a  $\pi$ -pulse time. We are considering that the bosonic modes,  $b$  and  $c$ , are initially in a thermal state where each of them contains 0.2 phonons [12]. In addition to the presence of the heating processes described by Eq. (20) with rates  $\Gamma_b \bar{N}_b \approx (2\pi) \times 133 \text{ Hz}$  and  $\Gamma_c \bar{N}_c \approx (2\pi) \times 9 \text{ Hz}$  (see appendix D), our simulations also include a Rabi frequency mismatch of 1%, and a trap frequency shift of 0.1%, and a constant energy shift of  $(2\pi) \times 20 \text{ kHz}$  on both ions.

For the second case, we also target the gates  $\exp(i\frac{\pi}{4}\sigma_1^z\sigma_2^z)$  and  $\exp(i\frac{\pi}{8}\sigma_1^z\sigma_2^z)$ , but now with a magnetic field gradient of  $300 \frac{\text{T}}{\text{m}}$ . Here, each gate is realised in a time of  $36.3 \mu\text{s}$ , i.e. 8 times the oscillation period of the com mode of the two-ion chain. Our operational regime is defined by the parameters  $\Omega \approx (2\pi) \times 10 \text{ MHz}$ ,  $\pi$ -pulse time of  $\approx 49 \text{ ns}$ ,  $\omega_2 - \omega_1 = (2\pi) \times 39.8 \text{ MHz}$  and while the energy shift upon the ions, errors on Rabi and trap frequencies, and the value of  $d$  are the same as in the previous case. The heating rates had to be recalculated leading to  $\Gamma_b \bar{N}_b \approx (2\pi) \times 248 \text{ Hz}$  and  $\Gamma_c \bar{N}_c \approx (2\pi) \times 16 \text{ Hz}$  (see appendix D). The initial states for the phonon modes coincide as well with the ones in the previous case.

The results are depicted in Table I, where a simple inspection reveals that, even under the error conditions we have included in the model, our method leads to fast two-qubit gates with fidelities exceeding 0.999. Finally, we want to note that the experimental achievement of higher values for  $g_B$  will re-

sult in faster gates without affecting significantly the reported fidelities.

## V. CONCLUSIONS

We have demonstrated that pulsed dynamical decoupling schemes are efficient generators of fast and robust two-qubit gates. The proposed microwave sequences can be implemented in hyperfine trapped-ion qubits driven with far-field radiation. Our gate scheme relies on a specifically designed microwave sequence that forces the two motional modes in a certain direction to cooperate, which makes the gate fast and robust against external noise sources including motional heating. This novel technique for the generation of quantum gates opens a path in the microwave control of trapped ions, which aligns with the efforts of scalability towards quantum supremacy in trapped-ion systems.

## ACKNOWLEDGEMENTS

This work was supported by the ERC Synergy grant BIOQ and the EU Projects EQUAM and DIADEMS and the SFB/TRR 21, Spanish MINECO/FEDER FIS2015-69983-P, Basque Government IT986-16 and PhD grant PRE-2015-1-0394. J. C. acknowledges Universität Ulm for a Forschungsbonus.

## APPENDIX A: The $^{171}\text{Yb}^+$ ion

In this appendix, we numerically argue that the presence of the additional hyperfine levels of the  $^{171}\text{Yb}^+$  ion, the fluctuations of the magnetic field, and the effect of fast rotating terms does not threaten the gate fidelities claimed in this article. For numerical simplicity we have considered a single four level system and looked for the fidelity of the propagator

after a sequence of 20  $\pi$ -pulses is applied. We find that the error (infidelity) is on the order of  $10^{-5}$ , hence being one order of magnitude below the gate errors reported in Table I. Therefore, we conclude that the presence of the additional levels, counter rotating terms, and the fluctuations of the magnetic field have a negligible effect on the final fidelity of the gate to the order claimed in this article. We detail now the parameters and conditions in our numerical simulations.

In the hyperfine ground state of the  $^{171}\text{Yb}^+$  ion, transitions can be selected with the appropriate polarization of the control fields. However, experimental imperfections might generate unwanted leakage of population from the qubit-states to other states. On the other hand, the presence of fluctuations of the magnetic field may also result in imperfect  $\pi$ -pulses which may also damage the performance of the gate. To account for these experimental imperfections we simulate the following 4-level Hamiltonian

$$\begin{aligned} H_{4l} = & E_0|0\rangle\langle 0| + E_1|1\rangle\langle 1| + E_2|2\rangle\langle 2| + E_3|3\rangle\langle 3| \\ & + X(t)|1\rangle\langle 1| - X(t)|3\rangle\langle 3| \\ & + \Omega(t)(|0\rangle\langle 1| + \epsilon|0\rangle\langle 2| + \epsilon|0\rangle\langle 3| + \text{H.c.}) \cos[\omega t + \phi(t)], \end{aligned} \quad (21)$$

where the energies of the hyperfine levels,  $E_i$ , are those corresponding to a  $^{171}\text{Yb}^+$  ion in a magnetic field of 100 G, and the qubit is codified in levels  $\{|0\rangle, |1\rangle\}$ . Function  $X(t)$  represents a fluctuating magnetic field, which shifts the magnetically sensitive levels  $|1\rangle$  and  $|3\rangle$  in opposite directions. Numerically we have constructed this function as an Ornstein-Uhlenbeck (OU) process [40], where the parameters have been chosen such that the qubit-levels, in the absence of any pulses, show a coherence decaying exponentially with a  $T_2$  coherence-time of 3ms, as experimentally observed [41]. Particularly, this corresponds to values  $\tau = 50 \mu\text{s}$  for the correlation time, and  $c = 2/(\tau * T_2)$  for the diffusion constant of the OU process.  $\Omega(t)$  is a step function taking exclusively values  $\Omega$  and 0, and  $\epsilon$  is a small number representing the leaking of the qubit population through unwanted transitions. For the numerical analysis we have used unfavourable values for this set of parameters. More specifically, the Rabi frequency was assigned a value of  $\Omega = (2\pi) \times 20\text{MHz}$ , which is already twice the maximum value used in all the other simulations throughout the article, having therefore a larger probability of exciting other hyperfine transitions. Moreover, the simulations were performed for the longest sequence discussed in the article, which lasts  $80 \mu\text{s}$ . We compare the propagator resulting from our simulations to the identity, which is what one would expect after an even number of  $\pi$ -pulses, 20 in our case, and we compute a value for the fidelity according to the definition

$$F_{A,B} = \frac{|\text{Tr}(AB^\dagger)|}{\sqrt{\text{Tr}(AA^\dagger)\text{Tr}(BB^\dagger)}}, \quad (22)$$

where  $F_{A,B}$  is the fidelity between operators  $A$  and  $B$ . To account for the stochastic effects of the OU process that models the fluctuations of the magnetic field, we have averaged the resulting fidelities over 100 runs of our numerical simulator. In

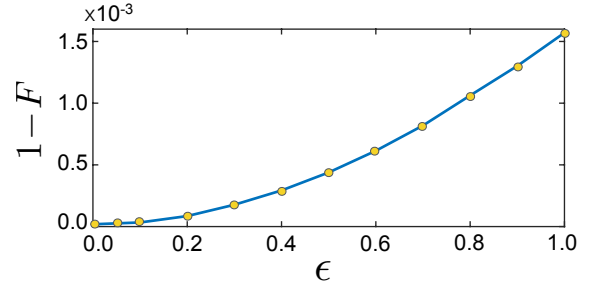


FIG. 5: Infidelity of an AXY-4 sequence, consisting of 20  $\pi$ -pulses and a total time of  $80\mu\text{s}$ , vs the strength of the leakage of population to other spectator levels. Each point is the average of the infidelities of 100 runs of the sequence in the presence of stochastic fluctuations of the magnetic field.  $\epsilon$  represent the strength of the transitions to unwanted levels in the hyperfine manifold of  $^{171}\text{Yb}^+$ , expressed in percentage with respect to the Rabi frequency of the transitions between the qubit-levels.

Fig. 5 we show the value of the infidelity,  $1 - F$ , for a number of values of  $\epsilon$ . We can see that the error grows non-linearly with the strength of the leakage due to polarisation errors of the control fields. However, for alignment errors below 20% ( $\epsilon = 0.2$ ) we obtain that the infidelity is smaller than  $10^{-4}$ . Hence, for polarisation errors below 20%, the effect of additional hyperfine levels, magnetic field fluctuations, and fast counter rotating terms should only be detectable in the fifth significant order of the gate fidelity, and not alter the 99.9% fidelity claimed in this article.

## APPENDIX B: Condition to make $G_{jm}(t) = 0$

In the following we show that  $G_{jm}(t) = 0$  when  $t$  is an even multiple of  $\tau$  such as at the end of the AXY-4 sequences and the frequency  $\nu_m = 2\pi r/\tau$  for  $r = 0, 1, 2, \dots$ . By the translation symmetry  $f_j(t' + 2\tau) = f_j(t')$ , we write the definition  $G_{jm}(2l\tau) = \int_0^{2l\tau} dt' f_j(t') e^{-i\nu_m t'}$  as  $G_{jm}(2l\tau) = \sum_{p=0}^{l-1} \int_0^{2\tau} dt' f_j(t') e^{-i\nu_m(t' + 2p\tau)}$  for  $l = 0, 1, 2, \dots$ . Using the condition that  $\nu_m \tau$  is a multiple of  $2\pi$ , we have  $G_{jm}(2l\tau) = lG_{jm}(2\tau)$ , where

$$\begin{aligned} G_{jm}(2\tau) &= \int_0^{2\tau} dt' f_j(t') e^{-i\nu_m t'} \\ &= G_{jm}(\tau) + \int_\tau^{2\tau} dt' f_j(t') e^{-i\nu_m t'} \\ &= G_{jm}(\tau) + \int_0^\tau dt' f_j(t' + \tau) e^{-i\nu_m(t' + \tau)} \\ &= G_{jm}(\tau) + \int_0^\tau dt' f_j(t' + \tau) e^{-i\nu_m t'}. \end{aligned} \quad (23)$$

Because of the anti-symmetric property of the AXY sequences  $f_j(\tau + t) = -f_j(t)$  we get  $G_{jm}(2\tau) = 0$  and hence  $G_{jm}(2l\tau) = 0$  for  $l = 0, 1, 2, \dots$ .



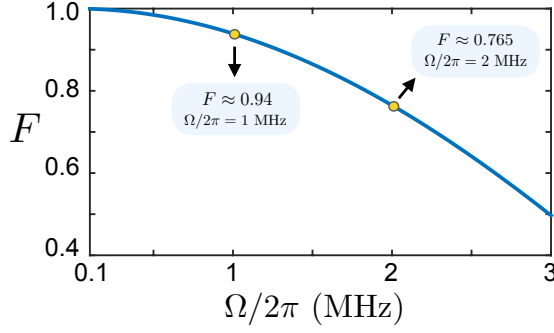


FIG. 6: Fidelity after 20  $\pi$ -pulses between the propagators associated to the Hamiltonians  $H = \frac{\Omega_1}{2}\sigma_1^{\phi_1} + \frac{\Omega_2}{2}[\sigma_2^+ e^{i\phi_1} e^{i\delta_2 t} + \text{H.c.}]$  and  $H = \frac{\Omega_1}{2}\sigma_1^{\phi_1}$  as a function of the Rabi frequency  $\Omega$ . We can observe how the fidelity decays because of the fail of the RWA. For this plot we have taken  $\delta_2 \approx (2\pi) \times 45$  MHz, a value that is even larger than the ones we will have our method based on  $\pi$ -pulses gets displayed.

### APPENDIX C: Pulse propagator

Our strategy to produce fast  $\pi$ -pulses on a certain ion qubit and, at the same time, eliminate undesired effects on the off-resonant qubit consists in appropriately choosing the Rabi frequency of the driving. When a  $\pi$ -pulse is applied, say on the first qubit, we have the following Hamiltonian

$$H = \frac{\omega_1}{2}\sigma_1^z + \frac{\omega_2}{2}\sigma_2^z + \Omega_1 \cos(\omega_1 t - \phi_1)(\sigma_1^x + \sigma_2^x). \quad (24)$$

In a rotating frame with respect to  $\frac{\omega_1}{2}\sigma_1^z + \frac{\omega_2}{2}\sigma_2^z$  and after eliminating fast rotating terms, the above Hamiltonian reads

$$H = \frac{\Omega_1}{2}\sigma_1^{\phi_1} + \frac{\Omega_2}{2}[\sigma_2^+ e^{i\phi_1} e^{i\delta_2 t} + \text{H.c.}], \quad (25)$$

where  $\sigma_1^{\phi_1} = \sigma_1^+ e^{i\phi_1} + \sigma_1^- e^{-i\phi_1}$  and  $\delta_2 = \omega_2 - \omega_1$ . At this level one can argue that, only when the Rabi frequency is small, the second term on the r.h.s. of the above equation is negligible. This unavoidably limits the value of  $\Omega_1$  and, consequently, how fast our decoupling pulses can be. In this respect, note that for a value of  $\omega_2 - \omega_1 \approx (2\pi) \times 45$  MHz, which is even larger than the ones used in see section IV, we find that  $\Omega_1$  should be significantly smaller than  $(2\pi) \times 1$  MHz if we want to eliminate the crosstalk between ions during 20  $\pi$ -pulses, see Fig. 6.

To eliminate this restriction, we can use the following expression

$$\begin{aligned} U_{[t:t_0]} &\equiv \hat{T} e^{-i \int_{t_0}^t H(s) ds} = U_0 \tilde{U}_{[t:t_0]} \\ &\equiv e^{-i H_\delta (t-t_0)} \hat{T} e^{-i \int_{t_0}^t U_0^\dagger (H(s) - H_\delta) U_0 ds}, \end{aligned} \quad (26)$$

where  $\hat{T}$  is the time ordering operator,  $H_\delta = -(\delta_2/2)\sigma_2^z$ , and find the time evolution operator for Eq. (25) in a generic time interval  $(t, t_0)$ . This is

$$U_{[t:t_0]} = e^{-i \frac{\Omega_1}{2} \sigma_1^{\phi_1} (t-t_0)} e^{i \frac{\delta_2}{2} \sigma_2^z (t-t_0)} e^{-i \gamma (t-t_0) \tilde{\sigma}_2}, \quad (27)$$

where  $\gamma = \frac{1}{2} \sqrt{\Omega_1^2 + \delta_2^2}$ ,

$$\tilde{\sigma}_2 = \frac{\Omega_1}{2\gamma} e^{i \frac{\delta_2}{2} t_0 \sigma_2^z} \sigma_2^{\phi_1} e^{-i \frac{\delta_2}{2} t_0 \sigma_2^z} + \frac{\delta_2}{2\gamma} \sigma_2^z. \quad (28)$$

Note that the first and the second terms in Eq. (25) commute, which allows to apply the relation (26) only to the part  $\frac{\Omega_1}{2}[\sigma_2^+ e^{i\phi_1} e^{i\delta_2 t} + \text{H.c.}]$ . Finally, for the sake of realising a  $\pi$ -pulse we will set  $(t - t_0) = t_\pi^{(1)} \equiv \frac{\pi}{\Omega_1}$  which gives rise to

$$U_{t_\pi}^{(1)} = e^{-i \frac{\Omega_1}{2} \sigma_1^{\phi_1} t_\pi} e^{i \frac{\delta_2}{2} \sigma_2^z t_\pi} e^{-i \gamma t_\pi \tilde{\sigma}_2}. \quad (29)$$

In the same manner, for a  $\pi$ -pulse (with  $t_\pi^{(2)} \equiv \frac{\pi}{\Omega_2}$ ) in resonance with the second ion we would have

$$U_{t_\pi}^{(2)} = e^{-i \frac{\Omega_2}{2} \sigma_2^{\phi_2} t_\pi} e^{i \frac{\delta_1}{2} \sigma_1^z t_\pi} e^{-i \gamma t_\pi \tilde{\sigma}_1}. \quad (30)$$

Equations (29) and (30) contain the  $\pi$ -pulses in which we are interested ( $e^{-i \frac{\Omega_1}{2} \sigma_1^{\phi_1} t_\pi}$  and  $e^{-i \frac{\Omega_2}{2} \sigma_2^{\phi_2} t_\pi}$ ) plus the crosstalk contributions we want to get rid off. To eliminate terms  $e^{-i \gamma t_\pi \tilde{\sigma}_2}$  and  $e^{-i \gamma t_\pi \tilde{\sigma}_1}$ , we will adjust the Rabi frequencies  $\Omega_{1,2}$  such that

$$\gamma t_\pi = \frac{1}{2} \sqrt{(\Omega_{1,2})^2 + (\delta_{2,1})^2} \frac{\pi}{\Omega_{1,2}} = \pi \times k, \text{ with } k \in \mathbb{Z}. \quad (31)$$

In this case we have that  $e^{-i \gamma t_\pi \tilde{\sigma}_2} = e^{-i \gamma t_\pi \tilde{\sigma}_1} = \pm 1$ , i.e. the unwanted terms contribute only as a global phase. Hence, only pure dephasing terms remain in both pulses,  $e^{i \frac{\delta_2}{2} \sigma_2^z t_\pi}$  and  $e^{i \frac{\delta_1}{2} \sigma_1^z t_\pi}$ , which will be cancelled by our tailored microwave sequences as explained in section IV.

### APPENDIX D: Heating rates estimation

To estimate the  $\Gamma_{b,c}$  parameters, we will rely on the data provided in [24] and by [42], as well as on the scaling relations one can extract from [39]. More specifically we take as reference values (for the com mode)  $\dot{n}_{\text{com}}^{\text{ref}} = 41$  phonons/second for a frequency  $\nu_1^{\text{ref}}/(2\pi) = 427$  kHz, and (for the breathing mode)  $\dot{n}_{\text{bre}}^{\text{ref}} = 7$  phonons/second for a frequency  $\nu_2^{\text{ref}}/(2\pi) = 459$  kHz, [24, 42]. The latter values correspond to a configuration at room temperature ( $T^{\text{ref}} = 300$  K) with an ion-electrode distance of  $d^{\text{ref}} \approx 310$   $\mu\text{m}$ , that would give rise to a magnetic field gradient  $g_B = 23.6 \frac{\text{T}}{\text{m}}$ .

Our operating conditions require, for the first studied case, an ion-electrode distance of  $d \approx 150$   $\mu\text{m}$ , to generate a magnetic field gradient of  $g_B = 150 \frac{\text{T}}{\text{m}}$  where  $\nu_1 = \nu$  and  $\nu_2 = \sqrt{3}\nu$  with  $\nu/(2\pi) = 150$  kHz, while we will consider low temperatures of  $T = 50$  K. In this situation one can derive new values for  $\dot{n}_{\text{com}}$  and  $\dot{n}_{\text{st}}$  using scaling relations [39] which in our case are

$$\dot{n}_{\text{com}} \approx \dot{n}_{\text{com}}^{\text{ref}} \left( \frac{\nu_1^{\text{ref}}}{\nu_1} \right)^2 \left( \frac{d^{\text{ref}}}{d} \right)^4 \left( \frac{T^{\text{ref}}}{T} \right)^{-2.13}, \quad (32)$$

and

$$\dot{n}_{\text{bre}} \approx \dot{n}_{\text{bre}}^{\text{ref}} \left( \frac{v_2^{\text{ref}}}{v_2} \right)^2 \left( \frac{d^{\text{ref}}}{d} \right)^4 \left( \frac{T^{\text{ref}}}{T} \right)^{-2.13}. \quad (33)$$

Then, one can use that, when close to the motional ground state, we have [39]

$$\dot{n}_{\text{com,bre}} = \Gamma_{b,c} \bar{N}_{b,c}, \quad (34)$$

that together with the definition of  $\bar{N}_{b,c} \equiv N_{b,c}^{\text{thermal}} = 1/(e^{\hbar\nu_{1,2}/k_B T} - 1)$ , allows us to obtain the values for  $\Gamma_{b,c}$ .

In the second studied case, a magnetic field gradient of  $g_B = 300 \frac{\text{T}}{\text{m}}$  would require to locate the ions closer to the electrodes, which would induce more heating. We estimate a distance according to the relation  $d = \sqrt{\frac{150}{300}} 150 \mu\text{m} \approx 106 \mu\text{m}$  that assumes a dependence  $g_B \sim \frac{1}{d^2}$ . This new distance can be used in Eqs. (32) and (33) to derive new values for the heating rates  $\Gamma_{b,c}$ .

- 
- [1] M. A. Nielsen and I. L. Chuang, *Quantum Computation and Quantum Information* (Cambridge University press, Cambridge, 2000).
  - [2] D. Leibfried, R. Blatt, C. Monroe, and D. Wineland, *Quantum dynamics of single trapped ions*, Rev. Mod. Phys. **75**, 281 (2003).
  - [3] H. Häffner, C. F. Roos, and R. Blatt, *Quantum computing with trapped ions*, Phys. Rep. **469**, 155 (2008).
  - [4] J. Casanova, A. Mezzacapo, L. Lamata, and E. Solano, *Quantum Simulation of Interacting Fermion Lattice Models in Trapped Ions*, Phys. Rev. Lett. **108**, 190502 (2012).
  - [5] A. Mezzacapo, J. Casanova, L. Lamata, and E. Solano, *Digital Quantum Simulation of the Holstein Model in Trapped Ions*, Phys. Rev. Lett. **109**, 200501 (2012).
  - [6] J. S. Pedernales, R. Di Candia, I. L. Egusquiza, J. Casanova, and E. Solano, *Efficient Quantum Algorithm for Computing n-time Correlation Functions*, Phys. Rev. Lett. **113**, 020505 (2014).
  - [7] I. Arrazola, J. S. Pedernales, L. Lamata, and E. Solano, *Digital-Analog Quantum Simulation of Spin Models in Trapped Ions*, Sci. Rep. **6**, 30534 (2016).
  - [8] C. J. Ballance, T. P. Harty, N. M. Linke, M. A. Sepiol, and D. M. Lucas, *High-Fidelity Quantum Logic Gates Using Trapped-Ion Hyperfine Qubits*, Phys. Rev. Lett. **117**, 060504 (2016).
  - [9] J. P. Gaebler, T. R. Tan, Y. Lin, Y. Wan, R. Bowler, A. C. Keith, S. Glancy, K. Coakley, E. Knill, D. Leibfried, and D. J. Wineland, *High-Fidelity Universal Gate Set for  $^9\text{Be}^+$  Ion Qubits*, Phys. Rev. Lett. **117**, 060505 (2016).
  - [10] T. Monz, P. Schindler, J. T. Barreiro, M. Chwalla, D. Nigg, W. A. Coish, M. Harlander, W. Hänsel, M. Hennrich, and R. Blatt, *14-Qubit Entanglement: Creation and Coherence*, Phys. Rev. Lett. **106**, 130506 (2011).
  - [11] F. Mintert, and C. Wunderlich, *Ion-Trap Quantum Logic Using Long-Wavelength Radiation*, Phys. Rev. Lett. **87**, 257904 (2001).
  - [12] S. Weidt, J. Randall, S. C. Webster, E. D. Standing, A. Rodriguez, A. E. Webb, B. Lekitsch, and W. K. Hensinger, *Ground-State Cooling of a Trapped Ion Using Long-Wavelength Radiation*, Phys. Rev. Lett. **115**, 013002 (2015).
  - [13] Ch. Piltz, T. Sriarunothai, S. S. Ivanov, S. Wölk, and Christof Wunderlich, *Versatile microwave-driven trapped ion spin system for quantum information processing*, Sci. Adv. **2** e1600093 (2016).
  - [14] T. P. Harty, M. A. Sepiol, D. T. C. Allcock, C. J. Ballance, J. E. Tarlton, D. M. Lucas, *High-Fidelity Trapped-Ion Quantum Logic Using Near-Field Microwaves*, Phys. Rev. Lett. **117**, 140501 (2016).
  - [15] M. B. Plenio, and P. L. Knight, *Decoherence limits to quantum computation using trapped ions*, Proc. Roy. Soc. A **453**, 2017 (1997).
  - [16] A. Khromova, Ch. Piltz, B. Scharfenberger, T. F. Gloger, M. Johanning, A. F. Varón, and Ch. Wunderlich, *Designer Spin Pseudomolecule Implemented with Trapped Ions in a Magnetic Gradient*, Phys. Rev. Lett. **108**, 220502 (2012).
  - [17] C. Ospelkaus, C. E. Langer, J. M. Amini, K. R. Brown, D. Leibfried, and D. J. Wineland, *Trapped-Ion Quantum Logic Gates Based on Oscillating Magnetic Fields*, Phys. Rev. Lett. **101**, 090502 (2008).
  - [18] C. Ospelkaus, U. Warring, Y. Colombe, K. R. Brown, J. M. Amini, D. Leibfried, and D. J. Wineland, *Microwave quantum logic gates for trapped ions*, Nature **476**, 181 (2011).
  - [19] N. Timoney, I. Baumgart, M. Johanning, A. F. Varón, M. B. Plenio, A. Retzker, Ch. Wunderlich, *Quantum gates and memory using microwave-dressed states*, Nature **476**, 185 (2011).
  - [20] A. Bermudez, P. O. Schmidt, M. B. Plenio, A. Retzker, *Robust trapped-ion quantum logic gates by continuous dynamical decoupling*, Phys. Rev. A **85**, 040302(R) (2012).
  - [21] D. Jonathan, M. B. Plenio, and P. L. Knight, *Fast quantum gates for cold trapped ions*, Phys. Rev. A **62**, 042307 (2000).
  - [22] R. Puebla, J. Casanova, and M. B. Plenio, *A robust scheme for the implementation of the quantum Rabi model in trapped ions*, New. J. Phys. **18**, 113039 (2016).
  - [23] R. Puebla, M.-J. Hwang, J. Casanova, and M. B. Plenio, *Protected ultrastrong coupling regime of the two-photon quantum Rabi model with trapped ions*, arXiv:1703.10539.
  - [24] S. Weidt, J. Randall, S. C. Webster, K. Lake, A. E. Webb, I. Cohen, T. Navickas, B. Lekitsch, A. Retzker, W. K. Hensinger, *Trapped-Ion Quantum Logic with Global Radiation Fields*, Phys. Rev. Lett. **117**, 220501 (2016).
  - [25] A. Sørensen and K. Mølmer, *Quantum Computation with Ions in Thermal Motion*, Phys. Rev. Lett. **82**, 1971 (1999).
  - [26] A. Sørensen and K. Mølmer, *Entanglement and Quantum Computation with Ions in Thermal Motion*, Phys. Rev. A **62**, 022311 (2000).
  - [27] I. Cohen, S. Weidt, W. K. Hensinger, and A. Retzker, *Multi-qubit Gate with Trapped Ions for Microwave and Laser-based Implementation*, New. J. Phys. **17**, 043008 (2015).
  - [28] D. F. V. James, *Quantum Dynamics of Cold Trapped Ions with Application to Quantum Computation*, Appl. Phys. B **66**, 181 (1998).
  - [29] B. Lekitsch, S. Weidt, A. G. Fowler, K. Mølmer, S. J. Devitt, C. Wunderlich, and W. K. Hensinger, *Blueprint for a Microwave Trapped Ion Quantum Computer*, Sci. Adv. **3**, e1601540 (2017).
  - [30] Supplemental Material
  - [31] S. Olmschenk, K. C. Younge, D. L. Moehring, D. N. Matsukevich, P. Maunz, and C. Monroe, *Manipulation and detection of a trapped  $\text{Yb}^+$  hyperfine qubit*, Phys. Rev. A **76** 052314 (2007).
  - [32] J. Casanova, Z.-Y. Wang, J. F. Haase, and M. B. Plenio, *Robust Dynamical Decoupling Sequences for Individual Nuclear Spin Addressing*, Phys. Rev. A **92**, 042304 (2015).
  - [33] Y. Wu, F. Jelezko, M. B. Plenio, and T. Weil, *Diamond Quantum Devices in Biology*, Angew. Chem. Int. Ed. **55**, 6586 (2016).
  - [34] Z.-Y. Wang, J. F. Haase, J. Casanova, and M. B. Plenio, *Positioning nuclear spins in interacting clusters for quantum technologies and bioimaging*, Phys. Rev. B **93**, 174104 (2016).
  - [35] J. Casanova, Z.-Y. Wang, and M. B. Plenio, *Noise-Resilient Quantum Computing with a Nitrogen-Vacancy Center and Nu-*

- clear Spins*, Phys. Rev. Lett. **117**, 130502 (2016).
- [36] Z.-Y. Wang, J. Casanova, and M. B. Plenio, *Delayed Entanglement Echo for Individual Control of a Large Number of Nuclear Spins*, Nat. Commun. **8**, 14660 (2017).
- [37] J. Casanova, Z.-Y. Wang, and M. B. Plenio *Arbitrary Nuclear Spin Gates in Diamond Mediated by a NV-center Electron Spin*, arXiv:1702.05330.
- [38] Ch. Piltz, B. Scharfenberger, A. Khromova, A.F. Varón, and Ch. Wunderlich, *Protecting Conditional Quantum Gates by Robust Dynamical Decoupling*, Phys. Rev. Lett. **110**, 200501 (2013).
- [39] M. Brownnutt, M. Kumph, P. Rabl, and R. Blatt, *Ion-trap measurements of electric-field noise near surfaces*, Rev. Mod. Phys. **87**, 1419 (2015).
- [40] D. T. Gillespie, *Exact numerical simulation of the Ornstein-Uhlenbeck process and its integral*, Phys. Rev. E **54**, 2084 (1996).
- [41] D. J. Wineland, C. Monroe, W. M. Itano, D. Leibfried, B. E. King, and D. M. Meekhof, *Experimental Issues in Coherent Quantum-State Manipulation of Trapped Atomic Ions*, J. Res. Natl. Inst. Stand. Technol. **103**, 259 (1998).
- [42] W. K. Hensinger (private communication).

## Supplemental Material: Fast and Robust Two-Qubit Gates with Microwave-Driven Trapped Ions

### VI. TWO HYPERFINE IONS UNDER A MAGNETIC FIELD GRADIENT

The Hamiltonian of the relevant hyperfine levels of the two qubit system (composed, in our case, of two  $^{171}\text{Yb}^+$  ions) under a  $z$  dependent magnetic field can be expressed as ( $\hbar = 1$ )

$$H = [\omega_e + \gamma B(z_1)]|e\rangle\langle e|_1 + \omega_g|g\rangle\langle g|_1 + [\omega_e + \gamma B(z_2)]|e\rangle\langle e|_2 + \omega_g|g\rangle\langle g|_2 + \nu_1 a^\dagger a + \nu_2 c^\dagger c, \quad (\text{S1})$$

where  $\gamma$  relates to the electronic gyromagnetic ratio as  $\gamma \equiv \frac{|g_e|}{2} \approx (2\pi) \times 1.4 \text{ MHz/G}$ , and  $B(z_j)$  is a position-dependent magnetic field that generates an additional energy splitting on the first ( $j = 1$ ) and second ( $j = 2$ ) ions. We have assumed that the ions, which interact through direct Coulomb force, perform only small oscillations around their equilibrium positions,  $z_j = z_j^0 + q_j$ . Under this assumption, Hamiltonian diagonalization yields frequencies  $\nu_1 = \nu$  and  $\nu_2 = \sqrt{3}\nu$ ,  $\nu$  being the axial trapping frequency, for the collective normal modes, namely the center-of-mass and breathing modes [S1].

If  $B(z_j)$  can be expanded to a good approximation to the first order in  $q_j$ , then  $B(z_j) = B_j + g_B q_j$ , where  $B_j \equiv B(z_j^0)$  and  $g_B \equiv \partial B / \partial z_j|_{z_j=z_j^0}$ . With this, and up to an energy displacement, the Hamiltonian (S1) reads

$$H = \frac{1}{2}[\omega_e + \gamma B_1 - \omega_g] \sigma_1^z + \frac{1}{2}[\omega_e + \gamma B_2 - \omega_g] \sigma_2^z + \nu_1 a^\dagger a + \nu_2 c^\dagger c + \frac{\gamma g_B}{2}(q_1 + q_2) + \frac{\gamma g_B}{2}(q_1 \sigma_1^z + q_2 \sigma_2^z), \quad (\text{S2})$$

where we have used the relations  $|e\rangle\langle e|_j = \frac{1}{2}(\mathbb{1} + \sigma_j^z)$  and  $|g\rangle\langle g|_j = \frac{1}{2}(\mathbb{1} - \sigma_j^z)$ . At this moment, it may be useful to recall that the displacement of the ions from their equilibrium positions,  $q_1$  and  $q_2$  can be expressed in terms of the collective normal modes,  $Q_1$  and  $Q_2$ , as

$$\begin{aligned} q_1 &= \frac{1}{\sqrt{2}}(Q_1 - Q_2) = \frac{1}{\sqrt{2}} \left[ \sqrt{\frac{\hbar}{2M\nu_1}}(a + a^\dagger) - \sqrt{\frac{\hbar}{2M\nu_2}}(c + c^\dagger) \right], \\ q_2 &= \frac{1}{\sqrt{2}}(Q_1 + Q_2) = \frac{1}{\sqrt{2}} \left[ \sqrt{\frac{\hbar}{2M\nu_1}}(a + a^\dagger) + \sqrt{\frac{\hbar}{2M\nu_2}}(c + c^\dagger) \right], \end{aligned} \quad (\text{S3})$$

$M$  being the mass of each ion. Using these relations, which follow the prescription in [S1], Eq.(S2) can be rewritten as

$$\begin{aligned} H &= \frac{1}{2}[\omega_e + \gamma B_1 - \omega_g] \sigma_1^z + \Delta_1(a + a^\dagger) \sigma_1^z - \Delta_2(c + c^\dagger) \sigma_1^z \\ &+ \frac{1}{2}[\omega_e + \gamma B_2 - \omega_g] \sigma_2^z + \Delta_1(a + a^\dagger) \sigma_2^z + \Delta_2(c + c^\dagger) \sigma_2^z \\ &+ \nu_1 a^\dagger a + \nu_2 c^\dagger c + \frac{\gamma g_B}{2} \sqrt{\frac{\hbar}{M\nu_1}}(a + a^\dagger), \end{aligned} \quad (\text{S4})$$

where we have defined  $\Delta_{1,2} \equiv \frac{\gamma g_B}{4} \sqrt{\frac{\hbar}{M\nu_{1,2}}}$  as the coupling strength between the qubits and the normal modes. The last term in

Eq.(S4) can be absorbed by a redefined bosonic operator  $b = a + \alpha$ , with  $\alpha = 2\Delta_1/\nu_1$ , which results in Hamiltonian

$$\begin{aligned} H = & \frac{1}{2} \left[ \omega_e - \omega_g - 2\alpha\Delta_1 + \gamma B_1 \right] \sigma_1^z + \Delta_1(b + b^\dagger) \sigma_1^z - \Delta_2(c + c^\dagger) \sigma_1^z \\ & + \frac{1}{2} \left[ \omega_e - \omega_g - 2\alpha\Delta_1 + \gamma B_2 \right] \sigma_2^z + \Delta_1(b + b^\dagger) \sigma_2^z + \Delta_2(c + c^\dagger) \sigma_2^z \\ & + \nu_1 b^\dagger b + \nu_2 c^\dagger c. \end{aligned} \quad (S5)$$

Finally, one can define  $\omega_{1,2} \equiv \omega_e - \omega_g - 2\alpha\Delta_1 + \gamma B_{1,2}$ , arriving at an expression for the system Hamiltonian of the form

$$H = \frac{\omega_1}{2} \sigma_1^z + \frac{\omega_2}{2} \sigma_2^z + \nu_1 b^\dagger b + \nu_2 c^\dagger c + \Delta_1(b + b^\dagger) \sigma_1^z - \Delta_2(c + c^\dagger) \sigma_1^z + \Delta_1(b + b^\dagger) \sigma_2^z + \Delta_2(c + c^\dagger) \sigma_2^z. \quad (S6)$$

## VII. THE TIME EVOLUTION OPERATOR

An analytical expression for the time evolution operator exists for any Hamiltonian of the form

$$H^I(t) = \sum_{j=1}^N \sum_{m=1}^M f_j(t) \Delta_{jm} (a_m e^{-i\nu_m t} + a_m^\dagger e^{i\nu_m t}) \sigma_j^z. \quad (S7)$$

The Hamiltonian for our ion system, undergoing a sequence of instantaneous  $\pi$ -pulses, is given by

$$\begin{aligned} H^I(t) = & f_1(t) \Delta_1 (b e^{-i\nu_1 t} + b^\dagger e^{i\nu_1 t}) \sigma_1^z - f_1(t) \Delta_2 (c e^{-i\nu_2 t} + c^\dagger e^{i\nu_2 t}) \sigma_1^z \\ & + f_2(t) \Delta_1 (b e^{-i\nu_1 t} + b^\dagger e^{i\nu_1 t}) \sigma_2^z + f_2(t) \Delta_2 (c e^{-i\nu_2 t} + c^\dagger e^{i\nu_2 t}) \sigma_2^z, \end{aligned} \quad (S8)$$

and therefore belongs to this category with  $a_1 = b$ ,  $a_2 = c$  and  $\Delta_{11} = \Delta_{21} = \Delta_1$ ,  $\Delta_{12} = -\Delta_{22} = -\Delta_2$ .

The time evolution operator of a time dependent Hamiltonian is given by the Dyson series or equivalently by the Magnus expansion:

$$U(t) = \exp \{ \Omega_1(t) + \Omega_2(t) + \Omega_3(t) + \dots \}, \quad (S9)$$

where (in general for  $t_0 \neq 0$ )

$$\begin{aligned} \Omega_1(t, t_0) &= -i \int_{t_0}^t dt_1 H(t_1) \\ \Omega_2(t, t_0) &= -\frac{1}{2} \int_{t_0}^t dt_1 \int_{t_0}^{t_1} dt_2 [H(t_1), H(t_2)] \\ \Omega_3(t, t_0) &= \frac{i}{6} \int_{t_0}^t dt_1 \int_{t_0}^{t_1} dt_2 \int_{t_0}^{t_2} dt_3 ([H(t_1), [H(t_2), H(t_3)]] + [H(t_3), [H(t_2), H(t_1)]]), \end{aligned} \quad (S10)$$

and so on. In our case,  $\Omega_k$  terms for  $k > 2$  are zero because  $[H(s), [H(s'), H(s'')]] = 0$ . The first term  $\Omega_1$  can be written as

$$\Omega_1(t, t_0) = -i \sum_{j,m} \Delta_{jm} [a_m G_{jm}(t, t_0) + a_m^\dagger G_{jm}^*(t, t_0)] \sigma_j^z \quad (S11)$$

where

$$G_{jm}(t, t_0) = \int_{t_0}^t dt' f_j(t') e^{-i\nu_m t'}. \quad (S12)$$

The second term can be calculated to be

$$\begin{aligned} \Omega_2(t, t_0) &= -\frac{1}{2} \int_{t_0}^t dt_1 \int_{t_0}^{t_1} dt_2 [H(t_1), H(t_2)] = -\frac{i}{2} \int_{t_0}^t dt_1 [H(t_1), \Omega_1(t_1, t_0)] \\ &= -\frac{i}{2} \int_{t_0}^t dt_1 \sum_{jm} \sum_{j'm'} (-i) \Delta_{jm} \Delta_{j'm'} [f_j(a_m e^{-i\nu_m t_1} + a_m^\dagger e^{i\nu_m t_1}) \sigma_j^z, (a_{m'} G_{j'm'} + a_{m'}^\dagger G_{j'm'}^*) \sigma_{j'}^z] \\ &= -\frac{i}{2} \int_{t_0}^t dt_1 \sum_{jj'} \sum_m (-i) \Delta_{jm} \Delta_{j'm} (f_j G_{j'm}^* e^{-i\nu_m t_1} [a_m, a_m^\dagger] + f_j G_{j'm} e^{i\nu_m t_1} [a_m^\dagger, a_m]) \sigma_j^z \sigma_{j'}^z \\ &= i \sum_m \int_{t_0}^t dt_1 \frac{1}{2i} \Delta_{1m} \Delta_{2m} (f_1 G_{2m} + f_2 G_{1m}) e^{i\nu_m t_1} \sigma_1^z \sigma_2^z + \text{H.c.} + K(t, t_0) \mathbb{1}, \end{aligned} \quad (S13)$$

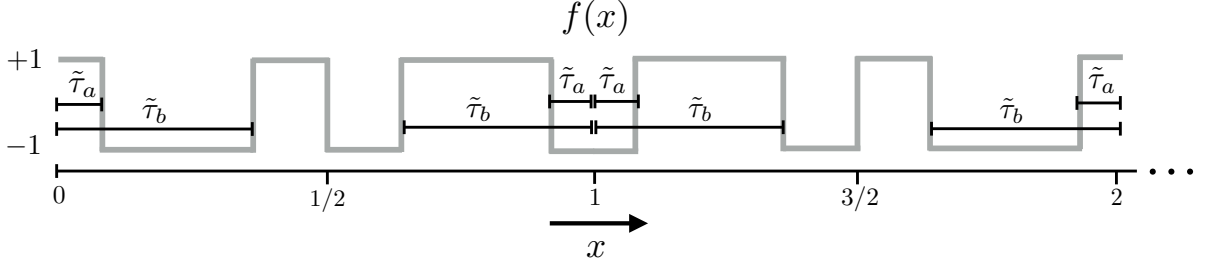


FIG. S1: Modulation function  $f(x)$  function that corresponds to the first two blocks of the AXY-4 pulse sequence. Time has been normalised by the characteristic time of the sequence  $\tau$  ( $x = t/\tau$ ), as well as  $\tilde{\tau}_a = \tau_a/\tau$  and  $\tilde{\tau}_b = \tau_b/\tau$ .

where, we have made use of  $[a_m, a_{m'}^\dagger] = \delta_{m,m'}$  and  $(\sigma_j^z)^2 = \mathbb{1}$ . In a more convenient manner,  $\Omega_2(t, t_0)$  can be expressed as

$$\Omega_2(t, t_0) = i\varphi(t, t_0)\sigma_1^z\sigma_2^z + K(t, t_0)\mathbb{1}, \quad (\text{S14})$$

where the phase  $\varphi$  is a time dependent function given by

$$\varphi(t, t_0) = \sum_m \int_{t_0}^t dt_1 \frac{1}{2i} \Delta_{1m} \Delta_{2m} \{f_1(t_1)G_{2m}(t_1, t_0) + f_2(t_1)G_{1m}(t_1, t_0)\} e^{i\nu_m t_1} + \text{H.c.}, \quad (\text{S15})$$

and we have ignored the term  $K(t)$ , as it will only contribute with a global phase. This can be equivalently written as

$$\varphi(t, t_0) = \sum_m \Im \int_{t_0}^t dt_1 \Delta_{1m} \Delta_{2m} \{f_1(t_1)G_{2m}(t_1, t_0) + f_2(t_1)G_{1m}(t_1, t_0)\} e^{i\nu_m t_1}, \quad (\text{S16})$$

where  $\Im$  indicates the imaginary part. Finally, we can easily check that the time evolution operator can be written as

$$U(t, t_0) = U_s(t, t_0)U_c(t, t_0) \quad (\text{S17})$$

where

$$U_s(t, t_0) = \exp \left\{ -i \sum_{j,m} \Delta_{jm} \left[ a_m G_{jm}(t, t_0) + a_m^\dagger G_{jm}^*(t, t_0) \right] \sigma_j^z \right\}, \quad (\text{S18})$$

and

$$U_c(t, t_0) = \exp \left[ i\varphi(t, t_0)\sigma_1^z\sigma_2^z \right]. \quad (\text{S19})$$

### VIII. EVALUATING THE $G_{jm}(t)$ AND $\varphi(t)$ FUNCTIONS

Searching for all different sequences that fulfill the conditions  $G_{jm}(T_f) = 0$  and  $\varphi(T_f) \neq 0$  gets easy if we identify which are the indispensable variables that define the problem. The sequence function  $f_1(t) = f_2(t) = f(t)$  is completely defined by the four parameters  $\tau_a, \tau_b, \tau$ , and  $M$ , for the case of an AXY- $M$  sequence. The duration of the sequence is of course only determined by two of them:  $\tau$  and  $M$  ( $T_f = M\tau$ ). It is useful to rescale the domain on the  $f$  function using  $\tau$ , the characteristic time of the sequence, as  $t = x\tau$ . Then, the property  $f(t + \tau) = -f(t)$  becomes  $f(x + 1) = -f(x)$ , and also  $\tau_a, \tau_b$  may be redefined as  $\tilde{\tau}_a = \tau_a/\tau$  and  $\tilde{\tau}_b = \tau_b/\tau$ . The AXY-4 sequence with this time rescaling is shown in Fig. S1. With this change of variable, the  $G_{jm}$  functions at a time  $T_f$  read

$$G_{jm}(T_f) = \int_0^{T_f} dt f(t) e^{-i\nu_m t} = \tau \int_0^M dx f(x) e^{-i\nu_m x/\tau}. \quad (\text{S20})$$

Now, if we relate  $\tau$  and  $\nu$  as

$$\nu\tau = 2\pi r \text{ with } r \in \mathbb{N}, \quad (\text{S21})$$

we can construct functions that are independent of the frequency  $\nu$  as

$$\tilde{G}_{j1}(T_f) \equiv \nu_1 G_{j1}(T_f) = \nu_1 \tau \int_0^M dx f(x) e^{-i2\pi r x} = 2\pi r \int_0^M dx f(x) e^{-i2\pi r x} \quad (\text{S22})$$

$$\tilde{G}_{j2}(T_f) \equiv \nu_2 G_{j2}(T_f) = \nu_2 \tau \int_0^M dx f(x) e^{-i2\pi \sqrt{3} r x} = 2\pi \sqrt{3} r \int_0^M dx f(x) e^{-i2\pi \sqrt{3} r x}. \quad (\text{S23})$$

The same procedure can be followed for the  $\varphi(t)$  function, that can be redefined in terms of  $\tilde{\varphi}_1(t)$  and  $\tilde{\varphi}_2(t)$  as

$$\varphi(t) = \left(\frac{\Delta_1}{\nu_1}\right)^2 \tilde{\varphi}_1(t) - \left(\frac{\Delta_2}{\nu_2}\right)^2 \tilde{\varphi}_2(t) = \left(\frac{\Delta_1}{\nu_1}\right)^2 \left(\tilde{\varphi}_1(t) - \frac{1}{3\sqrt{3}} \tilde{\varphi}_2(t)\right) = \left(\frac{\Delta_1}{\nu_1}\right)^2 \tilde{\varphi}(t), \quad (\text{S24})$$

where

$$\tilde{\varphi}_1(T_f) = (2\pi r)^2 \Im \int_0^M dx \int_0^x dy [f_1(x)f_2(y) + f_2(x)f_1(y)] e^{i2\pi r(x-y)} \quad (\text{S25})$$

$$\tilde{\varphi}_2(T_f) = (2\pi \sqrt{3} r)^2 \Im \int_0^M dx \int_0^x dy [f_1(x)f_2(y) + f_2(x)f_1(y)] e^{i2\pi \sqrt{3} r(x-y)}, \quad (\text{S26})$$

or

$$\tilde{\varphi}(T_f) = (2\pi r)^2 \Im \int_0^M dx \int_0^x dy [f_1(x)f_2(y) + f_2(x)f_1(y)] (e^{i2\pi r(x-y)} - \frac{1}{\sqrt{3}} e^{i2\pi \sqrt{3} r(x-y)}). \quad (\text{S27})$$

Now, it is clear that the functions  $\tilde{G}_{j1}(T_f)$ ,  $\tilde{G}_{j2}(T_f)$ , and  $\tilde{\varphi}(T_f)$ , only depend on  $\tilde{\tau}_a$ ,  $\tilde{\tau}_b$ ,  $M$  and  $r$ . Therefore, the functions plotted in Fig. (3) of the main text (corresponding to cases  $M = 4$ ,  $r = 1, 2, 3$ ), do not depend on parameters  $\nu_m$  and  $\Delta_m$ , but only on  $\tilde{\tau}_a$  and  $\tilde{\tau}_b$ .

---

[S1] D. F. V. James, *Quantum Dynamics of Cold Trapped Ions with Application to Quantum Computation*, Appl. Phys. B **66**, 181(1998).